Strain relief and disorder in commensurate water layers formed on Pd(111)

2012 J. Phys.: Condens. Matter 24 124102

(http://iopscience.iop.org/0953-8984/24/12/124102)

IOP PUBLISHING JOURNAL OF PHYSICS: CONDENSED MATTER
J. Phys.: Condens. Matter **24** (2012) 124102 (9pp) doi:10.1088/0953-8984/24/12/124102

Strain relief and disorder in commensurate water layers formed on Pd(111)

F McBride, A Omer, C M Clay, L Cummings, G R Darling and A Hodgson

Surface Science Research Centre, University of Liverpool, Liverpool L69 3BX, UK

Received 5 August 2011, in final form 31 October 2011
Published 6 March 2012
Online at stacks.iop.org/JPhysCM/24/124102

Abstract
Water adsorbs and desorbs intact on Pd(111), forming a hydrogen-bonded wetting layer whose structure we examine by low energy electron diffraction (LEED) and He atom scattering (HAS). LEED shows that water forms commensurate ($\sqrt{3} \times \sqrt{3}$)R30° clusters that aggregate into a partially ordered, approximately (7 × 7) superstructure as the layer completes. HAS indicates that the water layer remains disordered on a local (approximately 10 Å) scale. Based on workfunction measurements and density functional theory simulations we propose that water forms small, flat domains of a commensurate ($\sqrt{3} \times \sqrt{3}$)R30° water network, separated by disordered domain boundaries containing largely H-down water. This arrangement allows the water layer to adapt its density and relieve the lateral strain associated with adsorbing water in the optimum flat atop adsorption site. We discuss different possibilities for the structure of these domain walls and compare this strain relief mechanism to the highly ordered, large unit cell structures formed on surfaces such as Pt(111).

(Some figures may appear in colour only in the online journal)

1. Introduction

Water adsorbs rather weakly on many transition metal surfaces, the water–metal interaction being similar in strength to that of the water–water hydrogen bond [1]. As a result, the structure of these interfaces is determined by the balance between optimizing the water–water H bonding and the direct interaction between water and the metal. Experimental studies of the low temperature adsorption behaviour of water at metal single-crystal surfaces can provide a detailed test of the different models for water structures, and also of our ability to calculate and predict these H-bonding structures from first principles [2]. Establishing the reliability of such model calculations is particularly important for attempts to model bulk solid–water interfaces, since experimental probes give only limited information about water at buried interfaces and developing realistic models requires a detailed understanding of the adsorption behaviour at different surfaces.

For metal surfaces, experiments have established that the more inert surfaces, such as the close-packed faces of filled d-band metals (Cu, Au), do not wet, instead water forms 3D multilayer ice clusters and leaves the metal surface exposed [2–4]. On more chemically active transition metals [5, 6], such as Pt [7, 8], Pd [9–12], Ru [13–20] and Ni [21], or on open faces such as Cu(110) [22–25], water forms a stable first layer that has a slightly greater binding energy than in multilayer water clusters [1]. Although it was originally believed that first-layer water simply adopted a bulk ice, $I_h(0001)$ bilayer structure [26, 27], recent studies show that water optimizes both its hydrogen bonding network and the water–metal interaction in order to stabilize adsorption [1]. The resulting structures are highly specific to the surface involved and have a profound effect on the physical behaviour of the interface. In particular, the structure of the first layer determines both its ability to hydrogen-bond to a second water layer and the energy cost of restructuring the first-layer water to optimize bonding to a multilayer water film. Together these factors determine if the surface will wet to form a continuous uniform ice film, or alternatively will form 3D multilayer ice clusters on top of a tightly bound water

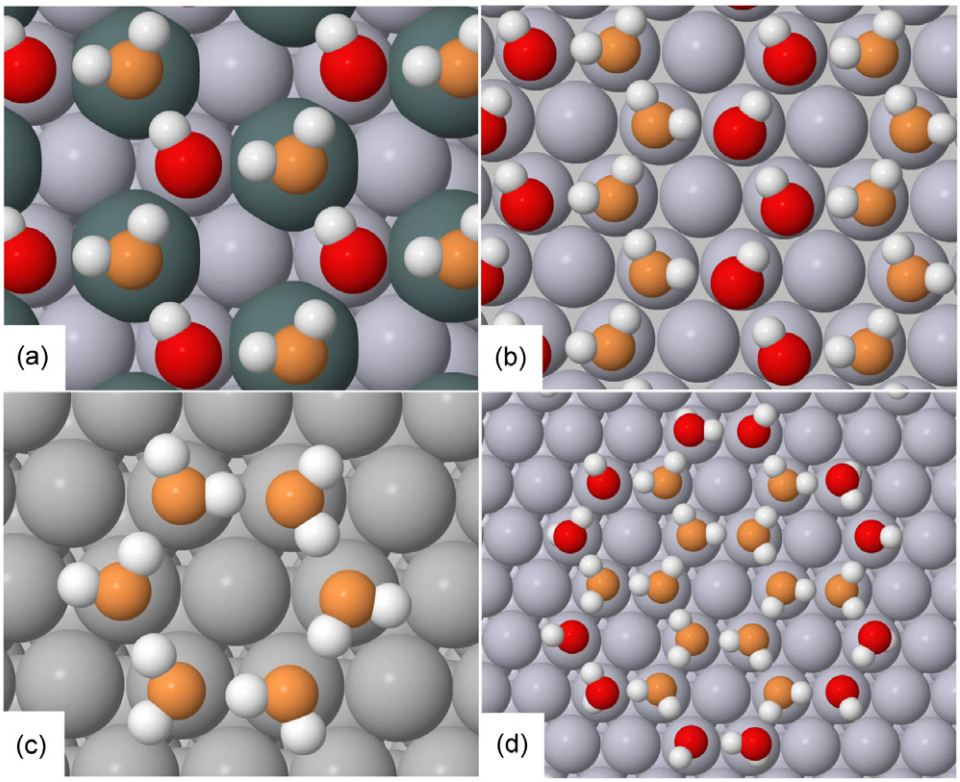

Figure 1. Calculated structures for different types of commensurate ice structures, shown with water bonded flat to the surface with O shaded orange (light grey) and O not bonded to the metal shaded red (dark grey). (a) The H-down ice bilayer formed by adsorption on the Pt(111)–($\sqrt{3} \times \sqrt{3}$) R30° Sn alloy template [32]. (b) Chains of flat and H-down water in a commensurate hexagonal network. (c) Flat water hexamer on Ru(0001) [41]. (d) Rosette formed on Pd(111) [9, 42].

monolayer [19, 21, 28–31]. Since the first layer of water plays such a key role in the description of the metal–water interface, there is great interest in understanding the H-bonding structures formed and how these depend on the properties of the particular surface [1].

Commensurate water layers were originally reported on many close-packed transition metal surfaces [26] and were believed to allow water to bind in a buckled, bilayer structure, with alternate O atoms in their favoured water adsorption site, atop the metal. However, a simple commensurate structure requires the lateral water–water separation to match the spacing of the metal surface, demanding a lateral expansion or compression of the water layer compared to bulk ice. New experiments suggest that the classic 'ice-like' bilayer, with a regular alternation in water adsorption geometry (figure 1(a)), is only formed when water is adsorbed on a suitable template, such as the corrugated SnPt(111) surface alloy which locks water into a ($\sqrt{3} \times \sqrt{3}$)R30° commensurate structure [32]. The lateral strain created in this commensurate water network is offset by the stabilization gained by adopting the favourable water binding site flat atop the Sn. Reports of simple commensurate structures on other surfaces were often caused by OH coadsorption, for example on Pt(111) [33] and Cu(110) [23], whereas in the absence of hydroxyl pure water forms complex structures with large unit cells, e.g. on Pt(111) [7, 8, 34–36], Ni(111) [21] and Cu(110) [23]. These complex structures are difficult to analyse experimentally, but it is known that water in the $\sqrt{39}$ layers formed on Pt(111) is adsorbed with the majority of the uncoordinated H atoms pointing down towards the metal surface [37]. Simulation of the STM images suggests that these structures form local regions of a commensurate flat hexagonal water network that is linked into a rotated H-down water network by five- and seven-membered rings [35]. This assignment is supported by vibrational spectroscopy [38] but, because of the large number of water molecules involved in these unit cells, their structures are difficult to define directly by experiment.

Two close-packed surfaces on which there is evidence for formation of commensurate water structures are Ru(0001) [39, 40] and Pd(111) [9–11]. The water–Ru(0001) system has received much attention, but is complicated by partial dissociation, although water does adsorb intact below approx. 150 K [17, 20]. Initially water forms small clusters of a hexagonal ($\sqrt{3} \times \sqrt{3}$)R30° network [41], allowing the majority of the water molecules to bind flat, atop the metal, figure 1(c). This arrangement optimizes the overlap between the $1b_1$ HOMO of water and the metal d_z orbital at the expense of a reduced average hydrogen bonding coordination. Only as the coverage is increased does the water form extended $\sqrt{3}$ hydrogen bonding networks, sacrificing some of the O–metal bonding as half of the water in the extended network loses contact with the metal surface to complete the 2D hydrogen bonding network. Helium atom scattering (HAS) shows that, despite the imposition of long range order on the O atom location by the hexagonal hydrogen bonding network, the water layer does not adopt a simple $\sqrt{3}$ periodicity [18].

Instead of a conventional ice bilayer, water appears to optimize the O–metal interaction by forming disordered chains or rings of water oriented flat and H-down within the overall water hydrogen bonding network (figure 1(b)). On Pd(111), STM studies [9, 42] show that water forms small 'rosettes' (figure 1(d)) and extended 'lace' structures at low temperature (100 K), consisting of a hexagonal network of water containing regular defects. DFT simulations indicate that these structures contain water bonded flat at the atop site, forming flat hexamer rings interlinked by flat and H-down oriented water molecules. These structures are metastable, with water aggregating into more compact structures as the surface is annealed to higher temperature [9], and it was concluded that formation of these flat networks was a kinetic, rather than a thermodynamic, effect.

In this study we examine the adsorption of water on Pd(111) using LEED and HAS measurements to compare with adsorption on Pt(111) and Ru(0001). We find that at low coverage water forms commensurate hexagonal structures that remain disordered on a larger scale as the coverage is increased. As the surface saturates and large islands form, the water layer forms an approx. (7 × 7) superstructure. We associate this structure with the ordering of anti-phase ($\sqrt{3} \times \sqrt{3}$)R30° water domains into an extended H-bonded superstructure. Despite the ordered LEED pattern, HAS indicates that the complete layer is disordered on a local scale. Based on workfunction measurements and DFT calculations we propose that the water layer consists of small, flat, commensurate ($\sqrt{3} \times \sqrt{3}$) R30° water domains, separated by disordered domain boundaries containing water that is mostly adsorbed H-down. Water in these structures is adsorbed primarily flat, parallel to the surface, or H-down. The domain structure allows water to adsorb in the favoured atop adsorption site whilst relieving the lateral strain associated with formation of an extended commensurate network and we compare this behaviour with the highly ordered, large unit cell structures formed on surfaces such as Pt(111).

2. Experimental details

Experiments were conducted in an ultra-high vacuum (UHV) chamber with a base pressure below 5×10^{-11} mbar. The main experimental chamber is equipped with a two-stage differentially pumped molecular beam for water dosing, a quadrupole mass spectrometer (QMS), HAS apparatus and a LEED system equipped with a dual microchannel plate (MCP) amplifier. The Pd(111) crystal, prepared to within ±0.25° of the (111) face, was welded directly to two Ta heating wires and connected via Ta posts to a liquid-nitrogen-cooled manipulator, allowing rapid heating and cooling of the crystal between 100 and 1000 K. Sample temperature was monitored via a K-type thermocouple, spot-welded to the back edge of the crystal. The sample was cleaned by repeated cycles of Ar^+ ion sputtering and annealing to 1000 K. Sample cleanliness was optimized using the water temperature programmed desorption (TPD), LEED and the helium atom reflectivity, the latter being particularly sensitive to surface contamination. Mounting the Pd crystal directly on the heating wires ensures that nothing except the sample desorbed gas during heating measurements, allowing the coverage and quality of the water layer to be accurately assessed.

Water films were grown using the effusive molecular beam, with a typical flux of 0.006 layers s^{-1}. A retractable flag was placed in front of the crystal, allowing the water dose to be controlled with a precision of better than 1%. The water coverage was calibrated relative to saturation of the first layer of water on the surface, θ_{sat}, using TPD measurements to provide an accurate endpoint for completion of the first layer. The relative coverage of water was then calculated from the desorption integral, with one layer corresponding to the coverage just before the appearance of a multilayer desorption peak in the TPD spectra, figure 1. The King and Wells direct reflection technique [43] was used to quantify water uptake from the beam, allowing the flux to be calibrated relative to θ_{sat}. Crystalline ice (CI) was grown at 140 K where water is sufficiently mobile to diffuse to its preferred adsorption sites, forming ordered 2D structures. The workfunction change associated with adsorption of the water layer was measured using a Kelvin probe to determine $\Delta\Phi$ as the water layer was desorbed from the surface.

HAS measurements were recorded at a fixed 90° total scattering angle by rotating the crystal [18]. Unless otherwise stated the measurements reported here were recorded for scattering along the [0 1 $\bar{1}$] scattering azimuth and a nozzle temperature of 300 K, corresponding to an energy, incident wavevector and energy resolution of $E = 65$ meV, $k_i = 11.1$ Å^{-1} and $\Delta E/E$ of 7.0% respectively. Previous LEED studies of water films on Pd(111) have shown significant restructuring after sustained exposure to the electron beam [44], so the beam current was kept <2 nA at all times and LEED patterns obtained for electron exposures between 1/20 and 1/100 electron/water showed no evidence of damage. Electron damage was observed when the exposures were deliberately increased by a factor of approx. 100, with evidence for desorption of water and, eventually, some dissociation to form OH. TPD measurements were always carried out after LEED or HAS to confirm the exact water coverage and check for dissociation. Experiments were repeated with H_2O and D_2O, but no differences were observed between the isotopes for adsorption on Pd(111).

DFT calculations were performed using the plane-wave basis set VASP code [45, 46]. The standard ultra-soft pseudopotentials were used for all atoms, and exchange and correlation were treated with the PW91 generalized gradient approximation [47]. A 3 × 3 × 1 Monkhorst–Pack [48] k-point set was used with a cutoff energy of 396 eV, a vacuum gap of 12 Å and dipole corrections were applied perpendicular to the surface. The accuracy of such calculations has been discussed elsewhere in relation to absolute binding energies and wetting behaviour [49, 50], but we note that similar DFT calculations have been shown to correctly reflect the relative stability of different intact and partially dissociated water structures, including, for example, on Ru(0001) [18, 49, 50] and Cu(110) [25, 51, 52]. On Pd(111) we find calculated adsorption energies for different structures (uncorrected for

Table 1. Calculated binding energies E_a and workfunction change $\Delta\Phi$ (relative to the clean surface) for different structures on Pd(111).

Structure	E_a (eV/water)	Coverage	$\Delta\Phi$ (eV)
$(\sqrt{3} \times \sqrt{3})$R30° H-up bilayer	0.50	0.67	−2.9
$(\sqrt{3} \times \sqrt{3})$R30° H-down bilayer	0.55	0.67	−0.25
$(2\sqrt{3} \times 2\sqrt{3})$R30° flat/H-down chains	0.61	0.67	−0.7
(7 × 7) Rosettes, figure 1(d)	0.58		
(6 × 6) figure 7(a)	0.62	0.67	−0.6
(7 × 7) figure 7(b)	0.59	0.71	−0.6
(7 × 7) figure 7(c)	0.59	0.71	−0.8
$(\sqrt{52}$R × $\sqrt{52})$R14°	0.61	0.81	−0.8
$(\sqrt{52}$R × $\sqrt{52})$R14°, figure 7(d)	0.62	0.73	−0.2

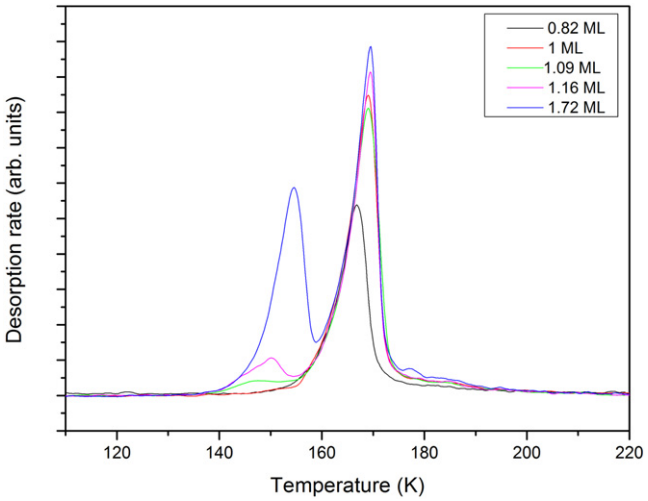

Figure 2. Water TPD as a function of initial coverage. Adsorption temperature was 140 K and the heating rate 0.8 K s^{-1}.

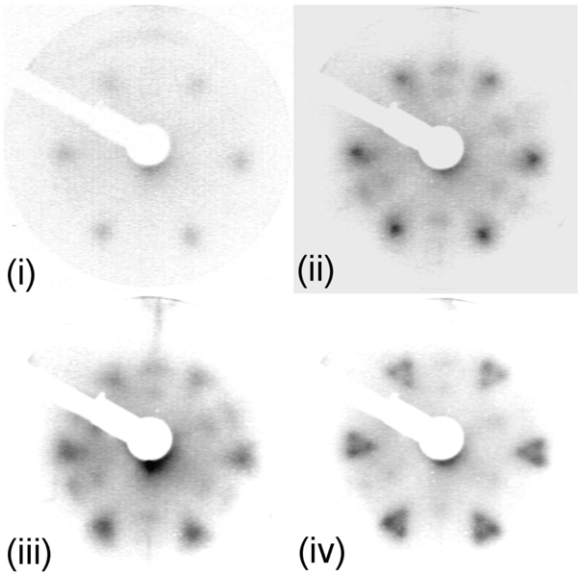

Figure 3. LEED images for an intact water film as a function of coverage showing the (1/3, 1/3) beams. (i) 0.67 layer, 56 eV, (ii) 0.88 layer, 50 eV, (iii) saturated water layer, 53 eV, and (iv) 1.5 layers, 53 eV. Adsorption temperature was 140 K throughout.

zero-point effects) of up to 0.62 eV/water (table 1), compared to a measured barrier to desorption of 0.51 eV/water.

3. Results and discussion

Thermal desorption of water from a clean Pd(111) surface occurs in two peaks, shown in figure 2, similar to the behaviour reported earlier [53]. The high temperature peak near 170 K saturates with increasing coverage and is due to water adsorbed in the first layer on Pd(111). This adsorption state follows pseudo-zero-order kinetics, with an activation barrier to desorption of 0.51 ± 0.04 eV, and is consistent with desorption from a dilute precursor state in equilibrium with dense 2D water islands. Saturation of the first-layer water desorption peak provides a convenient, reproducible reference point. The high temperature tail to the monolayer desorption peak is sensitive to the presence of steps, which stabilize water on the surface [54, 55], while a new peak near 190 K appears when the mixed OH + H_2O phase is formed by electron damage or reaction with O [44]. When the water dose is increased above one layer, a multilayer peak appears near 150 K and continues to grow indefinitely as the coverage is increased.

Figure 3 shows LEED images of the water films, recorded as a function of coverage after adsorption at 140 K. At all water coverages, from sub-monolayer up to several tens of layers of water, the film shows a $(\sqrt{3} \times \sqrt{3})$R30° LEED pattern with additional structure. For a water coverage of less than one layer, diffuse (1/3, 1/3) diffraction beams are observed, which become triangular in shape as the coverage is increased, with the points directed towards the adjacent integer order positions. In addition to the (1/3, 1/3) beams, a well-defined ring appears around the integer order beams, figure 4, and diffuse intensity can be seen either side of the (2 × 2) positions. When the water coverage is increased to the point where the first layer saturates, or above, the ordering becomes sufficient that the triangular (1/3, 1/3) diffraction beams split into three distinct maxima, leaving the intensity located at the corners of the original beam and no intensity in the (1/3, 1/3) position, figure 3(iv). Both the split (1/3, 1/3) beams and the ring around the integer order beams persist without change as several layers of water are deposited. Continued water adsorption results in slow degradation of the LEED pattern shown in figure 3(iv), but both the integer order metal beams and diffuse triangular (1/3, 1/3) adlayer beams remain visible up to coverages of approx. 80 layers of water. Since measurements on amorphous solid–water

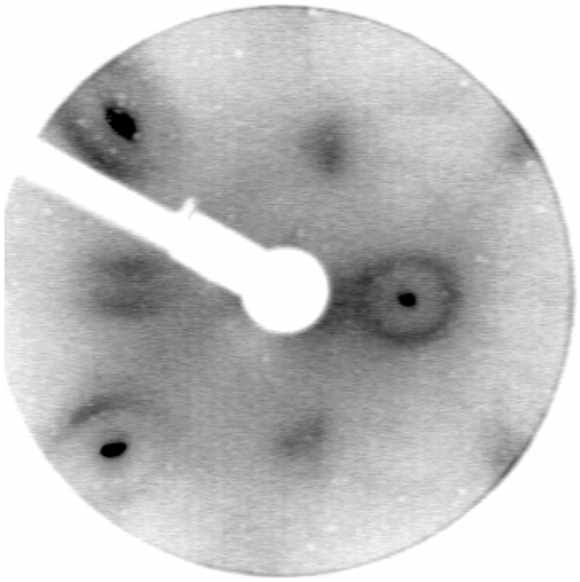

Figure 4. LEED pattern with the sample rotated away from the surface normal in order to view the diffuse rings appearing around the (0, 0) beam (centre right), with two metal spots visible left of the screen and the diffuse triangular $\sqrt{3}$ beams centre, top and bottom. Water coverage 1.5 layers, dosed at 140 K, beam energy 49 eV.

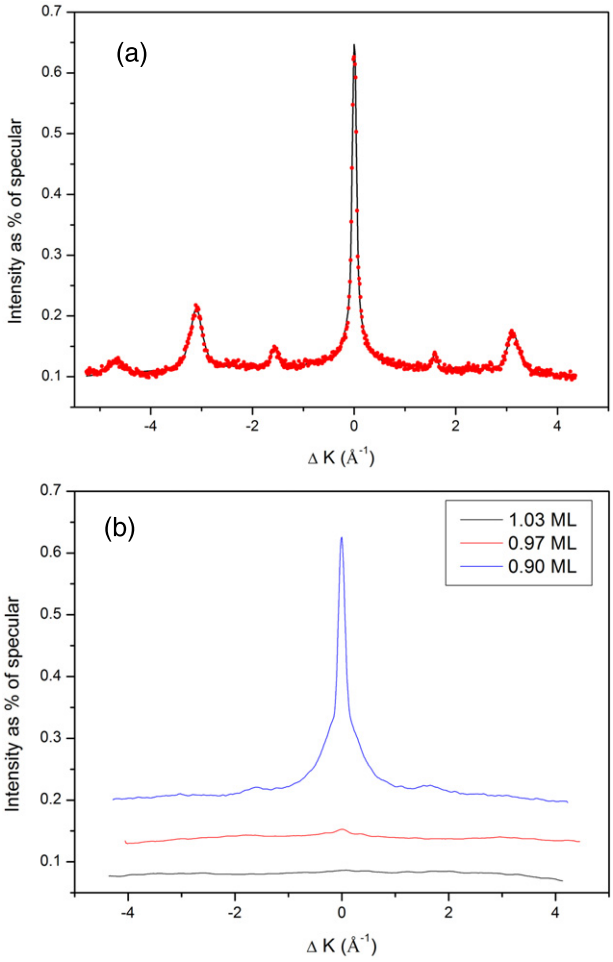

Figure 5. Helium atom scattering profiles for (a) a complete $(\sqrt{3} \times \sqrt{3})$R30° layer of the mixed (OH + H_2O) structure and (b) (top to bottom) 0.9, 0.97 and 1.03 layers of intact water adsorbed on Pd(111) at 140 K. The HAS data presented is for scattering along the [0 1 $\bar{1}$] azimuth at 100 K and $E = 65$ meV. Similar results were obtained at other beam energies.

films confirm the electron beam does not penetrate more than a couple of layers of water, the observation of sharp integer order diffraction beams indicates the multilayer water film is inhomogeneous, consisting of 3D water clusters and regions with a single water layer. This result is consistent with Kimmel *et al* [56] who found 3D clusters coexist with single-layer water on Pd(111).

In contrast with water networks such as the $\sqrt{39}$ structure found on Pt(111) [7, 34], the $2\sqrt{7}$ structure on Ni(111) [21] and the (7×8) structure formed on Cu(110) [23], which show all of the LEED diffraction beams associated with the large unit cell, adsorption on Pd(111) is dominated by the (1/3, 1/3) beam, with no evidence for any other sharp diffraction beams associated with a large, ordered unit cell. Electron scattering in LEED is dominated by the O atoms, and any consequent displacement of the surface Pd atoms, but is only indirectly sensitive to the H atom positions since scattering from H is weak. As an incomplete commensurate hexagonal $(\sqrt{3} \times \sqrt{3})$R30° network is observed at low temperatures in STM [9], it seems likely that the additional LEED structure is associated with anti-phase ordering of commensurate $(\sqrt{3} \times \sqrt{3})$R30° water domains. For example, formation of superstructure domain boundaries with a periodicity of approx. (7 ± 1) times the Pd lattice spacing would explain the observed splitting of the 1/3-order LEED beams and the size of the ring around the integer order spots. Based on the size of the beams in the split LEED pattern (e.g. figure 3(iv)), we estimate a coherent O domain size of approx. 80 Å or greater at high coverage.

In order to further probe the ordering of the water layer, HAS measurements were compared for a pure water layer and for the mixed (OH + H_2O) structure. Unlike electron scattering, which is sensitive only to the O and Pd positions, HAS is sensitive to the corrugation of the outermost layer, including any H atoms. The OH/H_2O layer consists of a coplanar, hexagonal $(\sqrt{3} \times \sqrt{3})$R30° network of O atoms with one H atom between each O, forming a hydrogen-bonded network with an intense LEED pattern and no additional superstructure [44]. HAS from the OH + H_2O structure shows intense high order diffraction peaks, figure 5(a), as expected from a highly corrugated, well-ordered commensurate phase. Changing K_i between 7 and 12.5 Å^{-1} made little difference to the intensity of the He diffraction peaks. In contrast, pure water layers behave quite differently in He scattering, figure 5(b). The intense specular He peak disappears progressively as water is adsorbed on the surface, with faint, broad scattering maxima appearing near the expected (1/3, 1/3) diffraction positions (± 1.7 Å^{-1}) before the layer saturates. However, both the broad scattering maxima and the specular peak disappear entirely as the first water layer is completed, leaving only a uniform background due to high angle scattering. Further water adsorption above a monolayer has no effect, but heating the surface to desorb

water immediately recovers the He reflectivity, confirming that a single water layer completely attenuates the coherent elastic scattering peak and that water desorbs intact to recover the bare metal surface.

The complete disappearance of coherent elastic He scattering from water on Pd(111) is a surprise, and is unlike the behaviour seen for HAS from water layers on other metal surfaces. For example, the $\sqrt{37}$ and $\sqrt{39}$ water layers formed on Pt(111) give sharp He diffraction patterns [8]. The water layer formed on Ru(0001) shows a sharp $\sqrt{3}$ LEED pattern and a sharp specular beam with broad HAS maxima [18, 57]. This behaviour is consistent with the O atoms adopting a well-defined lateral $\sqrt{3}$ ordering of the adsorption site, resulting in the LEED pattern, but disorder in the direction of the flat and H-down water chains within this network disrupting the corrugation and broadening the HAS peaks (see figure 1(b) and discussion in [18, 57]). The formation of split $\sqrt{3}$ LEED beams on Pd(111) indicates that, on this surface too, the O adsorption site maintains a $\sqrt{3}$ ordering, with anti-phase domains creating a splitting of the $\sqrt{3}$ beams. Based on the size of these split beams, the O location must be ordered over more than approx. 80 Å under high coverage conditions. In complete contrast, the absence of any coherent HAS intensity implies that the He-surface potential, which is sensitive to the electron density far from the surface, is disordered on a local scale. Based on typical cross sections for He atom scattering from surface adsorbates (of the order of 100 $Å^2$), the absence of any coherent fraction implies that the water layer is intrinsically disordered on a length scale of approx. 10 Å or less. This behaviour can be reconciled with the presence of an ordered LEED pattern if the water layer contains regions of an ordered $\sqrt{3}$ O network, separated by anti-phase domain boundaries, with disorder in the HAS originating from local disorder in the H orientation of some water molecules in the domain boundaries. The flat, tightly bound water that is adsorbed atop Pd is expected to have a lower Debye–Waller factor than the H bonded second-layer water, giving rise to a $\sqrt{3}$ LEED pattern, even when local disorder in the proton arrangement destroys coherent HAS [18, 57].

We can obtain some further constraint on the average orientation of the water layer by measuring the workfunction change, $\Delta\Phi$, as water is adsorbed on the surface, as shown in figure 6. The workfunction decreases linearly as the first water layer is deposited, with $\Delta\Phi = -0.70$ eV for the completed layer. Further growth to create an ice multilayer causes a progressively smaller change in $\Delta\Phi$ as 3D ice clusters form on the surface, the change in workfunction eventually saturating at $\Delta\Phi = -1.06$ eV.

In order to obtain some insight into the general structure of the water layer we carried out DFT simulations to determine what arrangements might be consistent with the experimental results, notwithstanding the disorder that is clearly intrinsic to this water layer. Initially the water was forced to adopt a simple commensurate arrangement, with water arranged in a hexagonal network, without any longer range superstructure such as indicated by LEED. A range of different possible structures were considered and table 1

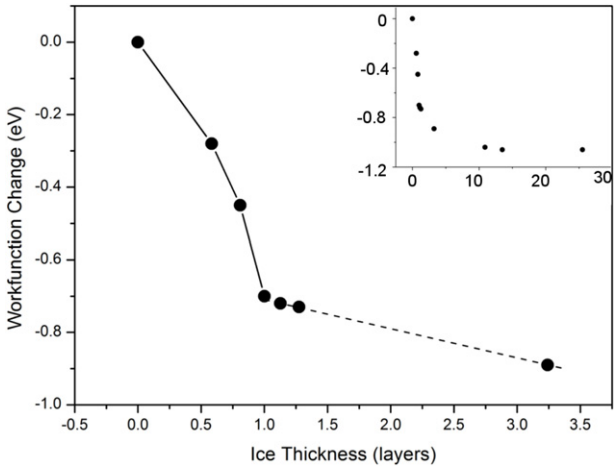

Figure 6. Workfunction change ($\Delta\Phi$) measured for a water film grown on Pd(111) at 140 K as a function of the water coverage. The dashed line and inset show the change in $\Delta\Phi$ from -0.7 eV as the first layer completes until $\Delta\Phi$ saturates at -1.06 eV for a thick water multilayer.

shows the calculated binding energies and workfunction change associated with several of these; the 'classic' $\sqrt{3}$ H-up or H-down bilayers (figure 1(a)), which have alternate water molecules bonded to the surface, and a structure (figure 1(b)) based on chains or rings of water molecules adsorbed flat atop Pd within an overall hexagonal hydrogen bonding network completed by H-down water molecules. The H-up and H-down bilayers have binding energies (0.50 and 0.55 eV) that are significantly lower than those of the chain structure (0.61 eV). Further support for the idea of a flat/H-down chain motif comes from the calculated workfunction change for this structure ($\Delta\Phi = -0.68$ V) which is very similar to the value ($\Delta\Phi = -0.70$ V) found experimentally, whereas the H-up and H-down bilayer structures have very different $\Delta\Phi$. Changing the arrangement of the flat and H-down water chains within the overall network, e.g. to form rings of flat water in the (6×6) structure shown in figure 7(a), slightly improves the binding energy and has minimal effect on the workfunction change, suggesting that the flat/H-down chain motif forms the basis for the observed water layer. The increased stability of these structures compared to the H-up/H-down bilayers mimics the behaviour found on Ru(0001) [41]. Formation of flat chains or rings allows half the water to bind close to the Pd, improving the interaction between its filled $1b_1$ orbital and the metal.

Whereas water on Ru(0001) forms a simple $\sqrt{3}$ structure at 0.67 ML coverage, LEED shows the layer formed on Pd(111) has an additional superstructure. Cerda *et al* [9] showed that growth at lower temperatures forms 'lace' or 'rosette' structures in which the majority of the water remains flat, in a double donor-single acceptor arrangement, bonded directly to the Pd. These arrangements are metastable and disappear at higher temperatures. DFT calculations did not find the flat structures, with their incomplete hydrogen bonding networks, to be any more stable than extended $\sqrt{3}$ bilayers. The rosette arrangement (figure 1(d)) has just one water in each outer hexagon of the rosette in a double acceptor

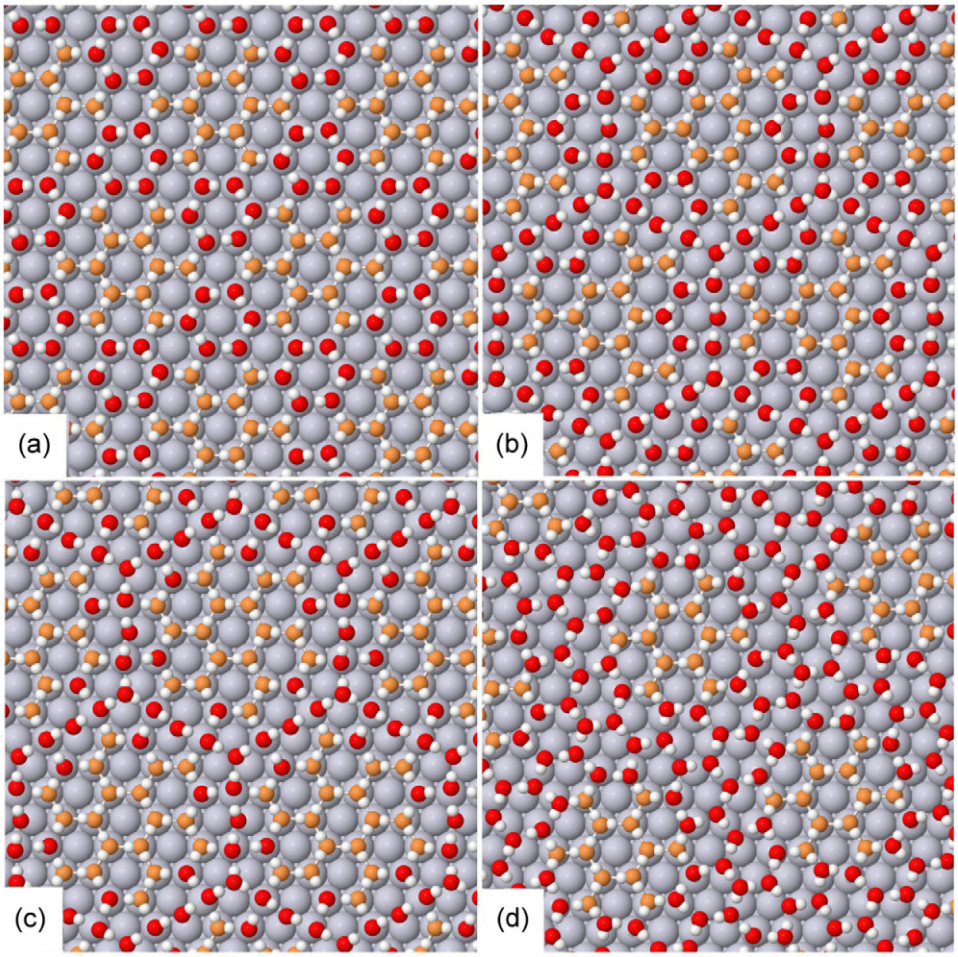

Figure 7. (a) A complete commensurate (6 × 6) water network formed from the rosette structure shown in figure 1(d); (b) and (c) a (7 × 7) unit cell with domain boundaries and a coverage of 0.71 ML; (d) a ($\sqrt{52} \times \sqrt{52}$)R14° structure with a coverage of 0.73 ML. The water molecules are colour-coded by the height of O above the surface, the orange (lighter grey) O atoms are for water bonded with $d_{\mathrm{O-Pd}} < 2.7$ Å, whereas red (darker grey) O atoms lie further from the surface.

geometry, completing the hydrogen bonding ring. We find the binding energy of the rosette structure (0.58 eV) is slightly larger than that of an extended $\sqrt{3}$ water bilayer, but less than that of the chain structures (figure 1(b)) or a complete (6 × 6) network formed by linking the rosettes (figure 7(a)). Although these commensurate chain or ring structures are relatively stable, they are not consistent with the split $\sqrt{3}$ beams seen in LEED.

Based on the workfunction change for the different types of network, and the observation of a split $\sqrt{3}$ LEED pattern, we also examined possible structures containing flat anti-phase $\sqrt{3}$ domains, bound tightly to Pd, within H-down water networks that complete some approx. 7× superstructure. As HAS shows that the water layer remains disordered on a local scale, it is probably unrealistic to look for a unique structure for this water layer, but we can get an idea of the energetic cost associated with forming anti-phase $\sqrt{3}$ domains from modelling possible structures by DFT. Since the H-down water molecules are not directly bound to the metal, they are free to relax away from the atop sites [18] or even form different sized rings, as on Pt(111) [35]. One way to achieve anti-phase $\sqrt{3}$ domains is to pack flat water rosette structures, which are observed at low temperature (figure 1(d)), into a suitable superstructure and complete the layer largely with H-down water. Figure 7 shows several possible arrangements of water in a (7 × 7) or a ($\sqrt{52} \times \sqrt{52}$)R14°unit cell, either of which would be consistent with the spot splitting observed by LEED. Although we investigated several possible arrangements of the compression domain boundaries, including mixtures of five- and sixfold rings, we did not consider the possible formation of Bjerrum defects [51, 58]. The most stable compression structure found in a $\sqrt{52}$ unit cell (figure 7(d)) has a coverage 10% higher than the commensurate (6 × 6) network of figure 7(a) and a similar binding energy. Analysis of the O–Pd binding distances shows that this $\sqrt{52}$ structure allows the six waters surrounding the central flat hexagon to bond substantially closer to the Pd than in the other structures. Structures based around H-down pentamer rings (figures 7(b) and (c)) did not appear to be intrinsically any more stable than those based on hexagons. We conclude that compression structures based around $\sqrt{3}$ domains of flat water are at least as stable as the best commensurate structure, and pack more water onto the surface. In the absence of a well-defined unit

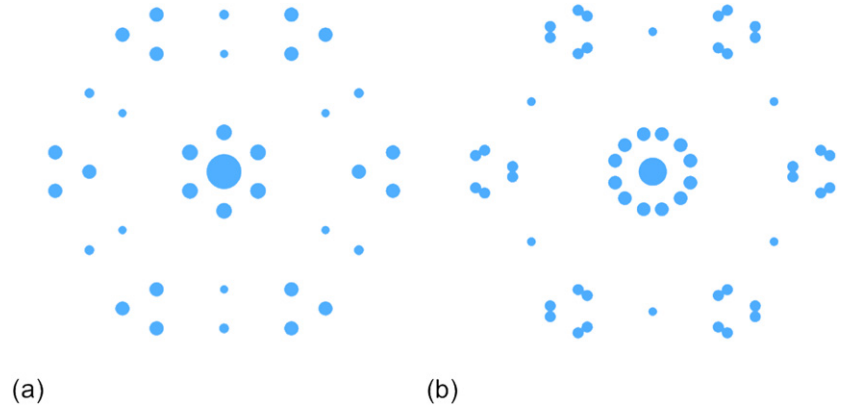

Figure 8. Simulation of the LEED patterns expected for (left) the (7 × 7) and (right) the $\sqrt{52}$ unit cells of figures 7(c) and (d). The spot size represents the calculated structure factor at 20 V, indicating the relative intensity expected for single scattering off the O atoms bonded directly to Pd. Additional weak LEED spots with an intensity less than 5% of the (0, 0) beam have been ignored for clarity. The simulations show a ring around the central (0, 0) beam and a splitting of intensity around the (1/3, 1/3) positions.

cell, DFT cannot distinguish between the different possible structures on energetic grounds alone. A simulation of the expected LEED pattern for the (7 × 7) and $\sqrt{52}$ structures (figures 7(c) and (d)) is shown in figure 8, assuming (following the arguments of [18]) that electron scattering is dominated by the water molecules that are bound flat above the Pd. Either unit cell reproduces the observed splitting of the $\sqrt{3}$ beams and the intensity around the integer order spots. In addition the simulations also predict intensity near the half-order positions, as observed in figure 3.

The formation of small, tightly bound commensurate domains of flat lying water, separated by domain boundaries containing H-down water, is in some ways similar to the arrangement recently proposed for the $\sqrt{37}$ and $\sqrt{39}$ structures formed on Pt(111) [35]. In that case the regions of flat, commensurate hexagonal water appear to be linked to a rotated hexagonal network of H-down water by three five- and three seven-membered rings, giving regions that image as dark threefold symmetric features in STM [35, 36]. Whereas the ordered structures formed on Pt(111) have a well-defined unit cell and show ordered LEED [29] and HAS [8], the layer formed on Pd(111) shows split (1/3, 1/3) diffraction beams but no well-defined long range superstructure. The complete absence of any coherent elastic HAS peak from the water layer, irrespective of the energy of the He atom beam, indicates this is not an interference effect but originates from disorder in the water structure. Evidently the disorder in the O positions, implied by the diffuse split LEED spots, and the resulting proton disorder, is sufficient to completely attenuate specular He scattering. This behaviour is qualitatively different from the behaviour on Ru(0001), where good long range order in the O location, but disorder in the water height, results in a diffuse HAS pattern from the highly corrugated surface [18]. The difference between these two situations appears to be associated with the formation of small flat networks of commensurate water on Pd(111), which partially order into anti-phase domains, whereas Ru(0001) retains longer range order, consistent with the formation of extended commensurate domains of flat or H-down water chains. This difference is likely associated with the change in lattice parameter and strain in the commensurate layer; the Ru spacing is 4% smaller than on Pd, allowing water to form extended flat commensurate networks. In the $\sqrt{52}$ structure shown in figure 7(d) the 12 central flat water molecules that are tightly bound to the Pd are contracted laterally by 3% compared to the Pd lattice, creating a strain in the water layer that hinders formation of an extended commensurate network and tips the energetic balance towards formation of out-of-phase domain boundaries.

4. Conclusion

Rather than adopting a simple commensurate structure, water adsorbed on Pd(111) forms a network containing regions of flat water, lying atop Pd in a ($\sqrt{3} \times \sqrt{3}$)R30° arrangement, separated by anti-phase domain boundaries with a periodicity of approx. 7 ± 1 units. The domain boundaries relieve the strain between commensurate flat water clusters and form from H-bonded rings of water, oriented mostly H-down, interacting only weakly with the surface. Although LEED shows there is order in the O locations, the layer does not form a precisely defined superstructure and HAS shows the layer remains disordered at a local level. This disorder is believed to reflect the small difference in binding energy between different arrangements of H-down water in the domain boundaries. The overall arrangement into regions of flat water, bonded tightly to the metal, within a loosely bonded H-down water network is related to the behaviour observed on both Ru(0001) [18], where the network remains commensurate, and Pt(111) where a well-defined large unit cell structure is formed [35], all of which appear to be driven by the formation of flat water structures within some extended H bonding network completed largely by H-down oriented water molecules.

Acknowledgment

We acknowledge EPSRC support of this work.

References

[1] Hodgson A and Haq S 2009 *Surf. Sci. Rep.* **64** 381
[2] Michaelides A and Morgenstern K 2007 *Nature Mater.* **6** 597
[3] Mehlhorn M and Morgenstern K 2007 *Phys. Rev. Lett.* **99** 246101
[4] Hinch B J and Dubois L H 1992 *J. Chem. Phys.* **96** 3262
[5] Schiros T, Takahashi O, Andersson K J, Ostrom H, Pettersson L G M, Nilsson A and Ogasawara H 2010 *J. Chem. Phys.* **132** 094701
[6] Shavorskiy A, Gladys M J and Held G 2008 *Phys. Chem. Chem. Phys.* **10** 6150
[7] Haq S, Harnett J and Hodgson A 2002 *Surf. Sci.* **505** 171
[8] Glebov A, Graham A P, Menzel A and Toennies J P 1997 *J. Chem. Phys.* **106** 9382
[9] Cerda J, Michaelides A, Bocquet M L, Feibelman P J, Mitsui T, Rose M, Fomin E and Salmeron M 2004 *Phys. Rev. Lett.* **93** 116101
[10] Yamada T, Okuyama H, Aruga T and Nishijima M 2003 *J. Phys. Chem.* B **107** 13962
[11] Wolf M, Nettesheim S, White J M, Hasselbrink E and Ertl G 1990 *J. Chem. Phys.* **92** 1509
[12] Gladys M J, El Zein A A, Mikkelsen A, Andersen J N and Held G 2008 *Surf. Sci.* **602** 3540
[13] Denzler D N, Wagner S, Wolf M and Ertl G 2003 *Surf. Sci.* **532** 113
[14] Denzler D N, Hess C, Dudek R, Wagner S, Frischkorn C, Wolf M and Ertl G 2003 *Chem. Phys. Lett.* **376** 618
[15] Weissenrieder J, Mikkelsen A, Andersen J N, Feibelman P J and Held G 2004 *Phys. Rev. Lett.* **93** 196102
[16] Tatarkhanov M, Fomin E, Salmeron M, Andersson K, Ogasawara H, Pettersson L G M, Nilsson A and Cerda J I 2008 *J. Chem. Phys.* **129** 154109
[17] Andersson K, Nikitin A, Pettersson L G M, Nilsson A and Ogasawara H 2004 *Phys. Rev. Lett.* **93** 196101
[18] Gallagher M, Omer A, Darling G R and Hodgson A 2009 *Faraday Discuss Chem. Soc.* **141** 231
[19] Haq S and Hodgson A 2007 *J. Phys. Chem.* C **111** 5946
[20] Clay C, Haq S and Hodgson A 2004 *Chem. Phys. Lett.* **388** 89
[21] Gallagher M, Omer A, Haq S and Hodgson A 2007 *Surf. Sci.* **601** 268
[22] Andersson K, Gomez A, Glover C, Nordlund D, Ostrom H, Schiros T, Takahashi O, Ogasawara H, Pettersson L G and Nilsson A 2005 *Surf. Sci.* **585** L183
[23] Schiros T, Haq S, Ogasawara H, Takahashi O, Öström H, Andersson K, Pettersson L G M, Hodgson A and Nilsson A 2006 *Chem. Phys. Lett.* **429** 415
[24] Yamada T, Tamamori S, Okuyama H and Aruga T 2006 *Phys. Rev. Lett.* **96** 036105
[25] Carrasco J, Michaelides A, Forster M, Haq S, Raval R and Hodgson A 2009 *Nature Mater.* **8** 427
[26] Thiel P A and Madey T E 1987 *Surf. Sci. Rep.* **7** 211
[27] Henderson M A 2002 *Surf. Sci. Rep.* **46** 5
[28] Kimmel G A, Petrik N G, Dohnálek Z and Kay B D 2005 *Phys. Rev. Lett.* **95** 166102
[29] Zimbitas G, Haq S and Hodgson A 2005 *J. Chem. Phys.* **123** 174701
[30] Zimbitas G and Hodgson A 2006 *Chem. Phys. Lett.* **417** 1
[31] Thürmer K and Bartelt N C 2008 *Phys. Rev. Lett.* **100** 186101
[32] McBride F, Darling G R, Pussi K and Hodgson A 2011 *Phys. Rev. Lett.* **106** 226101
[33] Clay C, Haq S and Hodgson A 2004 *Phys. Rev. Lett.* **92** 046102
[34] Harnett J, Haq S and Hodgson A 2003 *Surf. Sci.* **528** 15
[35] Nie S, Feibelman P J, Bartelt N C and Thurmer K 2010 *Phys. Rev. Lett.* **105** 026102
[36] Standop S, Redinger A, Morgenstern M, Michely T and Busse C 2010 *Phys. Rev.* B **82** 161412
[37] Ogasawara H, Brena B, Nordlund D, Nyberg M, Pelmenschikov A, Pettersson L G M and Nilsson A 2002 *Phys. Rev. Lett.* **89** 276102
[38] Feibelman P J, Kimmel G A, Smith R S, Petrik N G, Zubkov T and Kay B D 2011 *J. Chem. Phys.* **134** 204702
[39] Doering D L and Madey T E 1982 *Surf. Sci.* **123** 305
[40] Held G and Menzel D 1994 *Surf. Sci.* **316** 92
[41] Haq S, Clay C, Darling G R, Zimbitas G and Hodgson A 2006 *Phys. Rev.* B **73** 115414
[42] Tatarkhanov M, Ogletree D F, Rose F, Mitsui T, Fomin E, Maier S, Rose M, Cerda J I and Salmeron M 2009 *J. Am. Chem. Soc.* **131** 18425
[43] King D A and Wells M G 1972 *Surf. Sci.* **29** 454–82
[44] Clay C, Cummings L and Hodgson A 2007 *Surf. Sci.* **601** 562
[45] Kresse G and Furthmuller J 1996 *Phys. Rev.* B **54** 11169
[46] Kresse G and Hafner J 1993 *Phys. Rev.* B **47** 558
[47] Perdew J P, Chevary J A, Vosko S H, Jackson K A, Pederson M R, Singh D J and Fiolhais C 1992 *Phys. Rev.* B **46** 6671
[48] Monkhorst H J and Pack J D 1976 *Phys. Rev.* B **13** 5188
[49] Carrasco J, Santra B, Klimes J and Michaelides A 2011 *Phys. Rev. Lett.* **106** 026101
[50] Feibelman P J 2002 *Science* **295** 99
[51] Forster M, Raval R, Hodgson A, Carrasco J and Michaelides A 2011 *Phys. Rev. Lett.* **106** 046103
[52] Forster M, Raval R, Carrasco J, Michaelides A and Hodgson A 2012 *Chem. Sci.* **3** 93–102
[53] Wolf M, Nettesheim S, White J M, Hasselbrink E and Ertl G 1991 *J. Chem. Phys.* **94** 4609
[54] Nakamura M, Sato N, Hoshi N, Soon J M and Sakata O 2009 *J. Phys. Chem.* C **113** 4538
[55] Picolin A, Busse C, Redinger A, Morgenstern M and Michely T 2009 *J. Phys. Chem.* C **113** 691
[56] Kimmel G A, Petrik N G, Dohnalek Z and Kay B D 2007 *J. Chem. Phys.* **126** 114702
[57] Avidor N, Hedgeland H, Held G, Jardine A, Allison W, Ellis J, Kravchuk T and Alexandrowicz G 2011 *J. Phys. Chem.* A **115** 7205
[58] Feibelman P J 2005 *Chem. Phys. Lett.* **410** 120